THE ENERGY SPECTRUM OF ULTRA HIGH ENERGY COSMIC RAYS

Ioana C. Mariş for the Pierre Auger Collaboration

Institut für Experimentelle Kernphysik, Universität Karlsruhe (TH), Postfach 6980, Germany

The construction of the southern site of the Pierre Auger Observatory is almost completed. Three independent measurements of the flux of the cosmic rays with energies larger than 10^{18} eV have been performed during the construction phase. The surface detector data collected until August 2007 have been used to establish a flux suppression at the highest energies with a 6σ significance. The observations of cosmic rays by the fluorescence detector allowed the extension of the energy spectrum to lower energies, where the efficiency of the surface detector is less than 100% and a change in the spectral index is expected.

1 Introduction

Cosmic rays are particles that travel through the galactic and intergalactic space, arriving on Earth in a broad energy range up to 100 EeV. Their flux drops steeply with energy, from a few particles per second per m² up to one particle per km² per century at the highest energies. The shape of the flux depends on the evolution of the sources, the mechanisms that accelerate particles up to highest energies and the energy losses during the propagation of the particles from the sources to earth. The transition from galactic to extragalactic source is expected to be in the 0.1-5 EeV energy range. [1,2]

In the highest energy range, above 60 EeV, a flux suppression is expected due to the Greisen-Zatsepin-Kuzmin effect (GZK) [3,4] and/or due to the maximum energy that a cosmic ray accelerator can reach. The GZK suppression is a propagation effect: protons interact with the cosmic microwave background (CMB) radiation losing about 15% of their energy at each encounter with these CMB photons. Heavier elements are dissociated through photo-disintegration.

The previous experiments AGASA [5] and HiRes [6] have given contradictory results regarding the ultrahigh energy end of the energy spectrum where only indirect observations of cosmic rays are possible by the detection of extensive air showers. The previous measurements of the comic rays flux were dominated by statistical or systematic uncertainties. In order to decrease the uncertainties the Pierre Auger Observatory was built as a hybrid detector, combining the two techniques employed by the forerunner experiments: a surface detector array and a fluorescence detectors. Due to the hybrid technique the nearly calorimetric estimation of the energy of the primary particle as obtained from the fluorescence technique can be transfered to the large number of events recorded by the surface detector. Recently the flux suppression has been seen both by the Pierre Auger Observatory [7] and by the HiRes collaboration [6].

The observatory is described in the second section. The surface detector data are used to deduce the energy spectrum above 3 EeV where the trigger efficiency is 100%, as is described in the third section. Another complementary data set is delivered by the fluorescence detector itself. It can be used to extend the energy range down to 1 EeV. This measurement is described
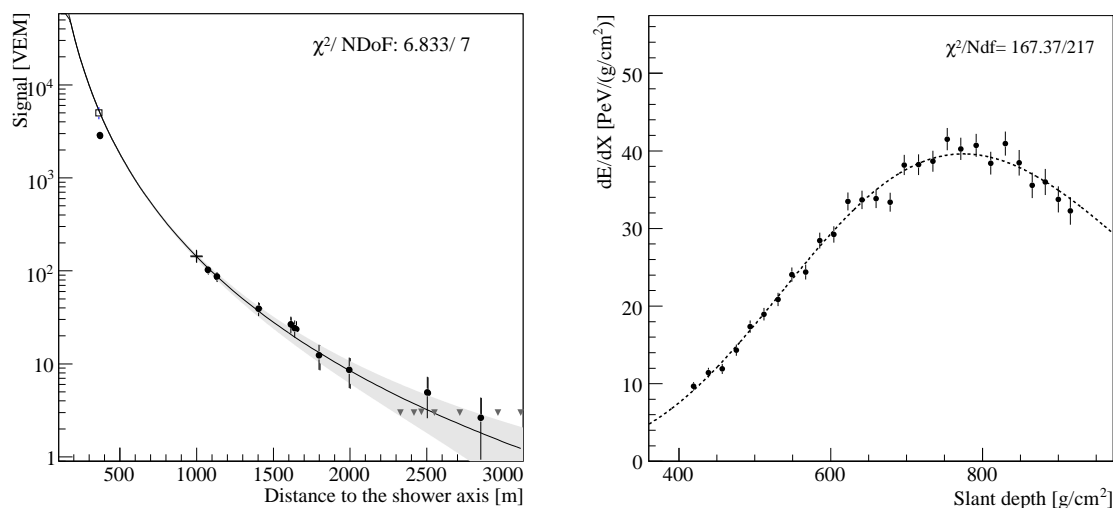
Figure 1: A typical golden hybrid event reconstruction, with an energy of 30 EeV and an incoming direction of 27° (left hand side) Lateral distribution. Filled circles represent acquired signals, triangles are functioning stations without signal used with Poisson probabilities in the maximum likelihood fit. S(1000) is marked with a cross. (right hand side) Longitudinal profile: energy deposit in the atmosphere as a function of the slant depth.

below in the last section together with the method of combining it with the surface detector flux estimate.

2 The Pierre Auger Observatory

After entering the atmosphere, cosmic rays interact with nuclei in the air and start creating extensive air showers. The charged particles that reach the ground are detected with the surface detector (SD), their lateral spread from the air shower axis at primary energies above 10^{18} eV is of the order of a few kilometers. On the way through the atmosphere charged particles excite nitrogen molecules, which afterwards emit fluorescence light in the ultra-violet band. The amount of light is proportional to the energy deposited by the air shower in the atmosphere.

The Pierre Auger Observatory, located in the province of Mendoza (Argentina), is utilized to measure the properties of extensive air showers by observing their longitudinal development in the atmosphere as well as their lateral spread at ground level. The Observatory consists of more than 1600 water-Cherenkov detectors, filled with 12 tonnes of water each and equipped with three photomultipliers to detect secondary photons and charged particles. The tanks are spread over about 3000 km^2 on a triangular grid of 1.5 km spacing. The atmosphere above the array is viewed by four fluorescence detectors (FD), each housing six telescopes, located on the border of the area. The field of view of each telescope is 30° in azimuth, and $1.5 - 30°$ in elevation. Light is focused with a spherical mirror of $11\,m^2$ effective area on a camera of 440 hexagonal pixels. Each pixel is a photomultiplier tube with 18 cm^2 detection area. More details on detector setup and calibration can be found in[8,9]. An extension of the Observatory has been started with AMIGA[10], a denser array of tanks equipped with muon counters which will lower the trigger threshold energy for the SD, and HEAT[11], three telescopes that will increase the field of view of FD up to 60°. The counterpart of the Southern side is in the planning phase in the Northern hemisphere, in Lamar, Colorado, which will provide large statistics above 50 EeV.

An example of a reconstruction of the same air shower with the SD and FD is shown in Fig. 1. The signals recorded in the tanks are converted in terms of vertical equivalent muons (VEM). One VEM represents the average of the signals produced in the 3 PMTs by a vertical
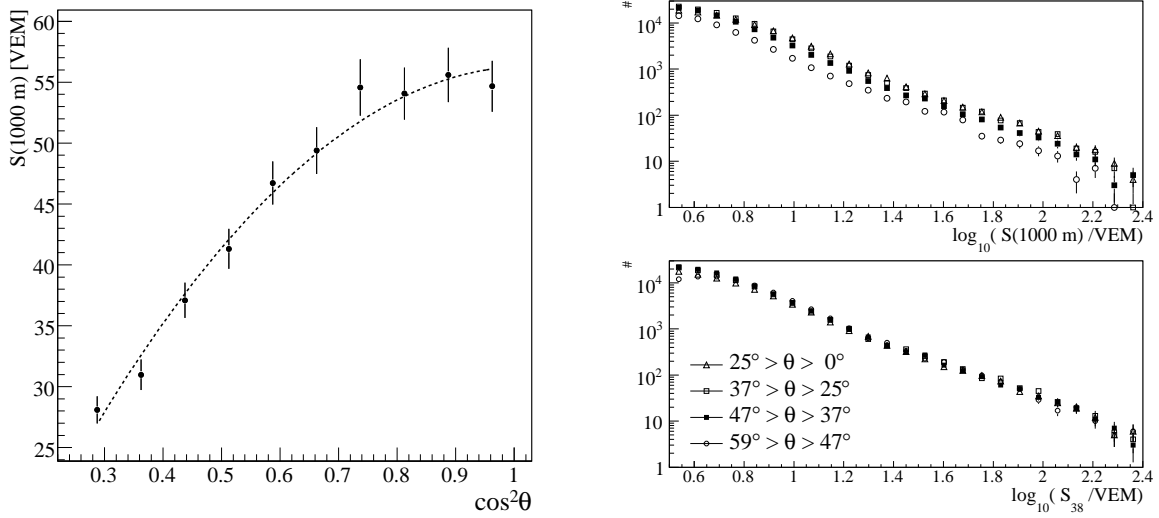
Figure 2: (left hand side) S(1000) attenuation in the atmosphere. The line represents an empirical fit that is used for the conversion to S_{38}.[7] (right hand side) The number of events as a function of S(1000) (upper panel) and as a function of S_{38}(lower panel) for equal $\cos^2(\theta)$ intervals.

muon that passes centrally through the SD detector. The air shower axis is obtained from the arrival time of the first particles in each detector station. The impact point on ground and the lateral distribution of signals are obtained in a global maximum likelihood minimization which accounts for the station trigger threshold and the overflow of the FADCs counts in the stations very close to the shower axis. The effect of the fluctuation of the lateral distribution function is minimized at 1000 m. This optimal distance is influenced by the array spacing. The signal at this specific distance, S(1000), is used as energy estimator [12].

About one in ten air showers that reach the surface detector are also observed with the fluorescence detector (the fluorescence detector operates only in moonless clear nights). The longitudinal profile of the air shower, i.e. the energy deposit as a function of traversed matter in the atmosphere is obtained taking into account the fluorescence and Cherenkov light contributions and the light scattering and attenuation [13]. Due to the limited field of view, the entire longitudinal profile usually is no recorded, so a fit with a Gaisser-Hillas function is employed to obtain the full profile. The energy of the cosmic ray is the integral over this function with a correction of $(10 \pm 5)\%$ for the energy carried away by the neutrinos and muons to which the FD is not sensitive. [14,15] The energy is proportional to the absolute fluorescence yield in air which at 293 K and 1013 hPa (337 nm band) is 5.05 ± 0.71 photons/MeV of energy deposited [16]. The fluorescence yield pressure and wavelength dependency are accounted for [17]. By using one triggered tank in the geometry reconstruction the accuracy is improved with respect to monocular data (i.e data recorded only by the fluorescence detector).

3 Energy spectrum from surface detector data

The lateral distribution of signals is a robust measurement, the only quality criteria required for the surface detector data is that the station that recorded the highest signal is surrounded by 6 active stations. This condition rejects events that might be affected by the array borders.

The reconstructed signal at 1000 m from the shower axis on the ground level, S(1000), is a good estimator for the energy of the cosmic ray. Due to the attenuation in the atmosphere, S(1000) depends on the zenith angle: an air shower developing vertically produces a smaller
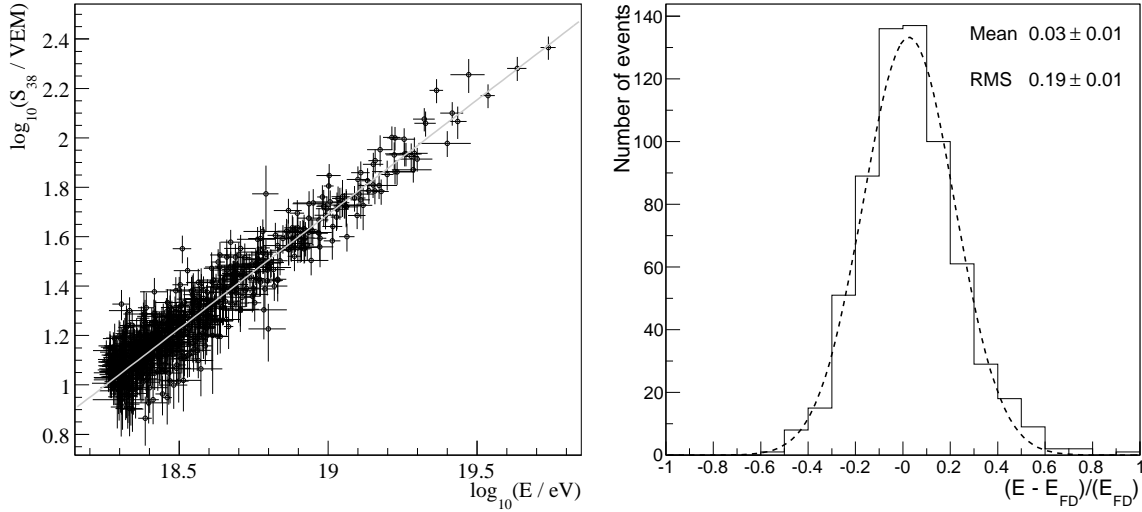
Figure 3: (left hand side) Energy calibration. The relation between S_{38} and energy is almost linear and is shown with the continuous line. (right hand side) The fractional difference between the assigned energy and the FD energy. [7]

signal than an inclined shower produced by a cosmic ray with the same energy. The constant intensity method [7] is exploited to obtain the zenith angle correction: it assumes that the cosmic ray flux is isotropic in local coordinates, i.e. the number of events above a certain threshold energy is constant as a function of $\cos^2 \theta$. This hypothesis leads to the correction function for S(1000) shown in Fig. 2(left). It is a second degree polynomial $S(1000)(x) = S_{38} \cdot (1 + a \cdot x + b \cdot x)$ where $x = \cos^2 \theta - \cos^2 38°$, $a = 0.94 \pm 0.06$ and $b = -1.21 \pm 0.27$. The quantity obtained by using the empirical fit shown in the same figure, S_{38}, represents the signal at $1000\,\mathrm{m}$ the very same shower would have produced if it had arrived from a zenith angle of $38°$. This angle corresponds to the median of the zenith angle distribution of the SD data. The number of events above a certain S_{38} is zenith angle independent. In principle the attenuation might be energy dependent, because showers with higher energies develop deeper in the atmosphere and can be observed before their maximum development. This effect was found to be negligible. Distributions of the number of events for equal $\cos^2 \theta$ intervals as a function of S(1000) and S_{38} are shown in Fig. 2 (right). After applying the correction function the zenith angle dependence disappears.

The transformation from S_{38} to energy is obtained by so called golden hybrid events. These are air showers that triggered both the SD array and the FD. Only a subsample of high quality FD measurements is used for the energy calibrations: For example the reduced χ^2 for the fit is required to be less than 2.5, data are selected only if measurements of the vertical aerosol optical depth are available and the maximum of the shower development is required to be in the field of view of the detector. Moreover, only events with a fraction of Cerenkov contribution of less than 50% of the total light, an uncertainty on the position of the shower maximum smaller than $40\,\mathrm{g/cm^2}$ and a relative total energy uncertainty less than 20% are used in the calibration procedure.

The relation between S_{38} and the FD energy is shown in Fig. 3 (left). As can be seen, it exhibits a power law correlation with a relative dispersion of $19 \pm 1\%$ (Fig. 3 (right)). The uncertainties in the determination of both FD energy and SD signal are assigned on an event by event basis. The energy uncertainty ($\approx 8\%$) includes also propagated atmosphere uncertainties and uncertainties from the air shower geometry reconstruction. The S_{38} uncertainty($\approx 16\%$)
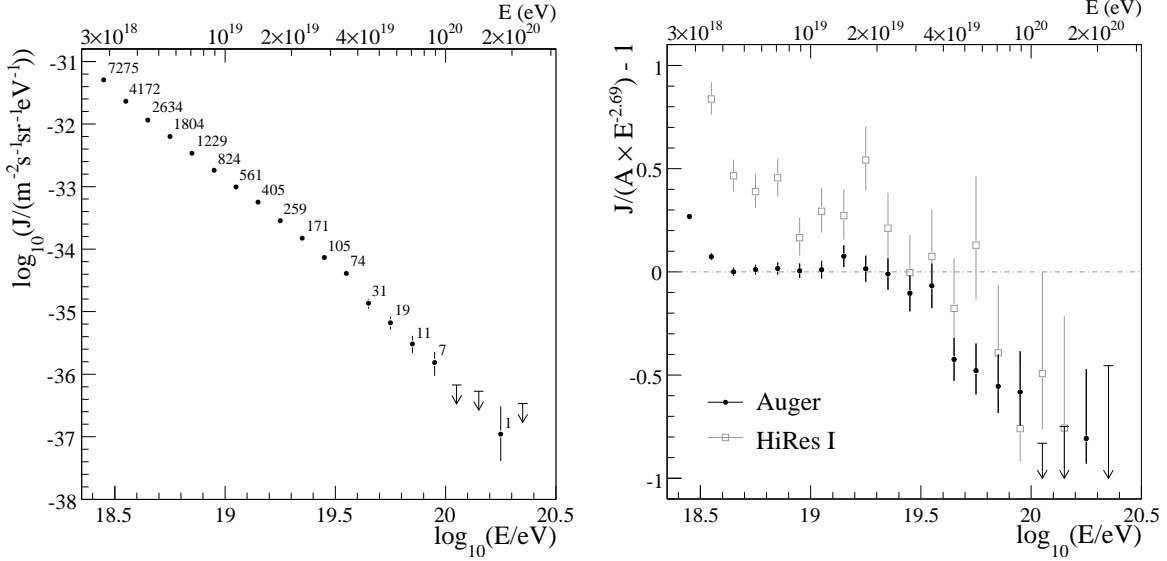
Figure 4: (left hand side) The differential flux as a function of energy. Also shown are the number of events in each bin. (right hand side) The fractional difference between the Auger vertical and HiRes I data and a spectrum with an index of 2.69 [7].

contains the lateral distribution function assumption, the shower to shower fluctuation and reconstruction accuracies. The best fit gives the transformation from S_{38} to energy as $E = A \cdot S_{38}^B$, $A = 1.49 \pm 0.06(\text{stat}) \pm 0.12(\text{sys})[10^{17} eV]$ and $B = (1.08 \pm 0.01(\text{stat}) \pm (0.04)(\text{sys}))$ with a reduced χ^2 of 1.1.

The spectrum built from $2 \cdot 10^4$ events recorded until August 2007 is shown in Fig. 4. The acceptance is computed by simple geometrical considerations and from the continuous monitoring of the configuration of the array [18]. The data set used for obtaining the energy spectrum contains only events with energies greater than $3 \cdot 10^{18}$ eV, since only above this energy the array is fully efficient. Due to reconstruction and trigger efficiency issues only events with a zenith angle of less than 60° are included in analysis. The integrated exposure for this period is $7 \cdot 10^3$ km^2 sr yr. The uncertainty of the acceptance is less than 5%. Having a duty cycle of almost 100 % the vertical spectrum from the SD has the lowest statistical and systematic uncertainties.

In Fig. 4 (right) the fractional difference between the vertical spectrum and a power-law $\propto E^{-2.69}$ is illustrated. Two spectral features are clearly visible: the so-called *ankle* at energies of $\approx 10^{18.5}$ eV and a flux suppression at energies above $\approx 10^{19.6}$ eV. A continuation of the spectrum as a power law with index 2.69 at highest energies predicts 167 ± 3 events above $10^{19.6}$ eV and 35 ± 1 above 10^{20} eV, whereas we observe only 69 events and 1 event. The hypothesis of a pure power-law can be rejected with a significance of 6 standard deviations, independent of the energy scale uncertainties.

4 The Auger spectrum: combining the hybrid and surface detector measurements

Air showers measured by the SD array with a zenith angle between 60° and 80° are used to determine an independent spectrum. The procedure to derive the energy is equivalent to the vertical events, but instead of using S_{38} the shower size is determined from the relative distributions of the two-dimensional muon number densities at ground level [19]. The normalization factor of the muon map, N_{19}, gives the total number of muons relative to a shower initiated by a proton with an energy of 10^{19} eV. The relation between N_{19} and the hybrid energy is shown
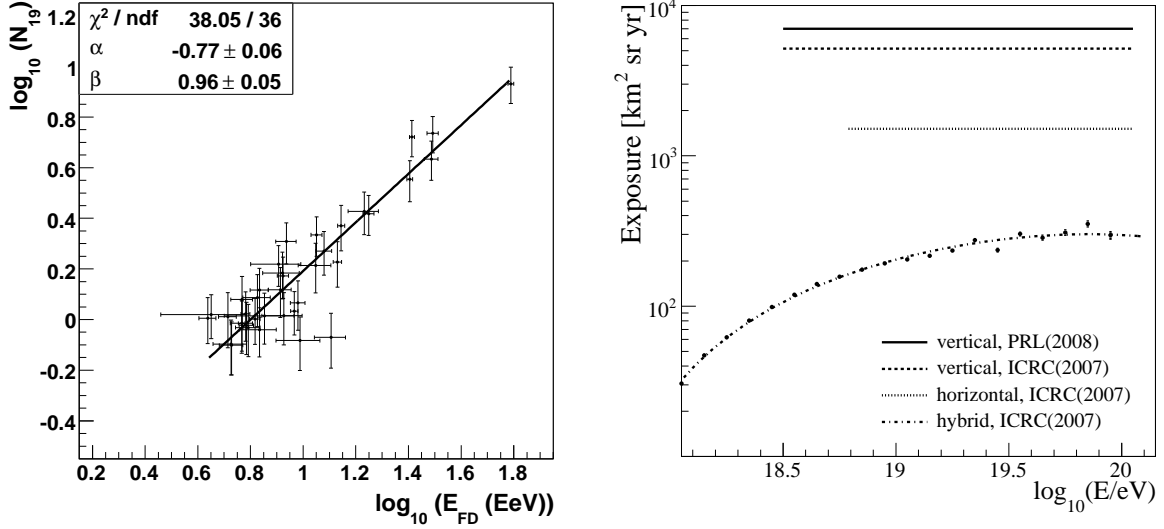
Figure 5: (left hand side) The energy calibration for the surface detector events with zenith angle between $60°$ and $80°$. (right hand side) The exposure for the three data sets used to determine the cosmic ray flux.

in Fig. 5. The statistics is rather low compared to the vertical energy calibration, but a clear almost linear dependency is seen.

The acceptance calculation for this set of events is purely geometrical and the threshold energy above which the trigger efficiency is more than 98% is $6.3 \cdot 10^{18}$ eV. Above this energy the integrated exposure until the end of February 2007 is $1510 \, \text{km}^2$ sr yr; 29% of the equivalent acceptance for vertical events [19].

Another data set available to measure the cosmic ray flux contains hybrid events. The hybrid exposure calculation relies on an accurate simulation of the fluorescence detector and the atmosphere. A large sample of Monte Carlo simulations are performed to reproduce the exact conditions of the experiment and the entire sequence of given configurations, from camera pixels to the combined SD-FD data taking of the observatory. The rapidly growing array, as well as the seasonal and instrumental effects are reproduced in the simulations within $10 \, \text{min}$ time intervals. The systematic uncertainty in the hybrid spectrum is currently dominated by the calculation of the exposure and reaches 20% in the low energy range. The advantage of the hybrid measurement of the energy spectrum [20] is the coverage of the energy range between 10^{18} eV and $3 \cdot 10^{18}$ eV.

The exposure for the three data sets is illustrated in Fig. 5. The hybrid measurement extends to the lowest energy range. Including the use of inclined SD data improve the statistics noticeably as this set has about a quarter of the event totals of the vertical data set in the highest energy region.

All spectra are affected by the 22% uncertainty in the FD energy scale, the main contributions coming from the determination of the fluorescence yield (14%). The profile reconstruction itself contributes with 10%. The absolute calibration of the telescopes is done every few months and has a contribution of 9.5%. The correction from the vertical aerosol optical depth measurements is 5-18%, giving an uncertainty on the energy of 4%. The advantage of the hybrid energy determination over the only SD assignment (e.g. as in the case of AGASA experiment) is that the uncertainties are experimentally driven and can be improved. A single surface detector experiment determines the primary cosmic ray energy with the help of simulations of air showers therefore the uncertainties are driven by theoretical uncertainties which are harder to decrease.
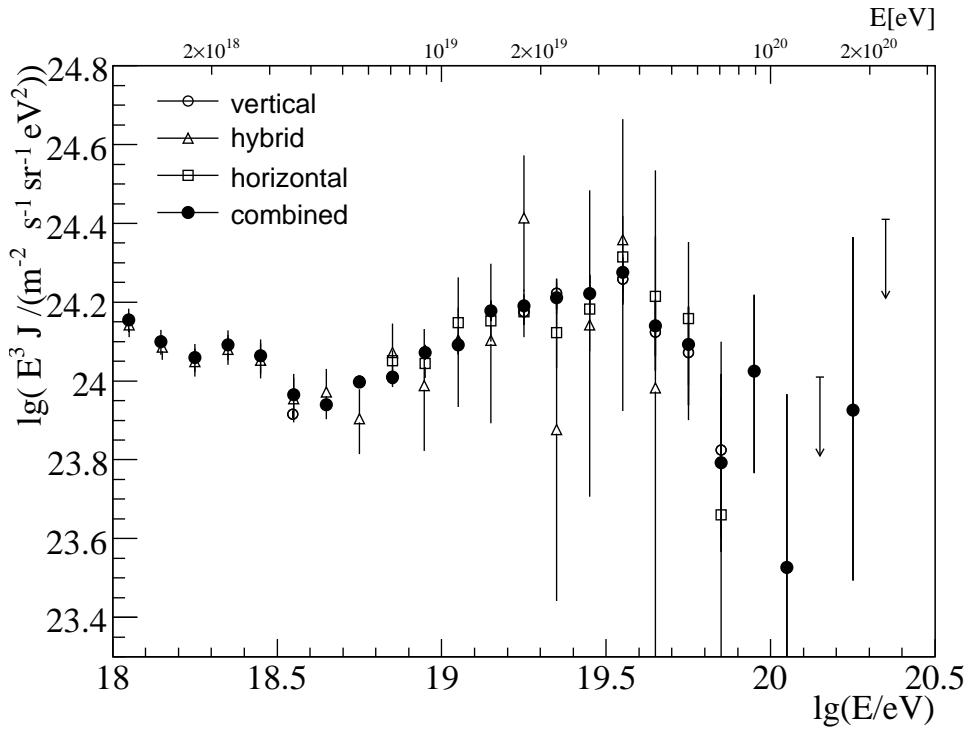
Figure 6: The energy spectra obtained at the Pierre Auger Observatory as presented in [21]. The combined spectrum is shown with filled circles. Open circles represent the energy spectrum obtained from events with a zenith angle of less than 60°, triangles represent the hybrid measurement and open squares the energy spectrum obtained from surface detector data with a zenith angle between 60° and 80°. Only statistical uncertainties are shown.

The energy spectra obtained with the three methods are illustrated in Fig. 6. The systematic uncertainty of the energy does not affect the relative comparison of the three spectra. The agreement is well within the independent systematic uncertainties, the difference between the overall normalizations is at a level of less than 4%.

The Auger combined differential flux, shown in the same figure multiplied with the third power of energy, is extending over the widest energy range possible and with minimal uncertainties. To deduce the spectrum a maximum likelihood method is applied taking into account the independent uncertainties of each measurement. [21] The combined spectrum is dominated by the vertical surface detector measurement above $3\,\mathrm{EeV}$ and by the hybrid spectrum in the lower energy range. The spectral index changes from $\gamma_1 = -3.30 \pm 0.06$ to $\gamma_2 = -2.69 \pm 0.02(\mathrm{stat}) \pm 0.06(\mathrm{sys})$ at $\log(E_{\mathrm{ankle}}/\mathrm{eV}) = 18.65 \pm 0.04$, and above $10^{19.6}\,\mathrm{eV}$ to $\gamma_3 = -4.2 \pm 0.4(\mathrm{stat})$.

5   Conclusions

The energy spectrum has been measured at the Pierre Auger Observatory with three independent data sets and the agreement is better than 4%.

A flux suppression at the highest energies has been established with a significance of 6 standard deviations. Combined with the recent result that the highest energy cosmic rays are anisotropic and a good correlation only with relatively nearby sources has been found[22], it hints towards a GZK effect.

A change of the spectral index occurs at about $4\,\mathrm{EeV}$ which might indicate either the transition from galactic to extragalactic origin of cosmic rays or a propagation effect. To distinguish between the models a determination of the mass of the cosmic rays[23] over the entire energy range is necessary. The exact location of the spectral index change and an accurate measurement of the spectrum below $3\,\mathrm{EeV}$ will be possible in the near future with AMIGA and HEAT extensions of the observatory.

The exact shape of the energy spectrum in the highest energy range, which can be used to distinguish between acceleration scenarios[21], will be determined with greatly improved precision over the next 10 years of data taking.

References

1. V. Berezinsky *et al.*, *Nucl. Phys. (Proc. Suppl.)* **151**, 497 (2006).
2. D. Allard *et al.*, submitted to *Astron. Astrophys.*(2007), astroph/0703633.
3. K. Greisen, *Phys. Rev. Lett.* **16**, 748 (1966).
4. G.T. Zatsepin and V.A. Kuz'min, *JETP Lett.* **4**, 78 (1966).
5. M. Takeda *et al.*, *Astropart. Phys.* **19**, 447 (2003).
6. R.U. Abbasi *et al.*, *Phys. Rev. Lett.* **100**, 101101 (2008).
7. J.Abraham *et al.* [Pierre Auger Collaboration] accepted in *Phys. Rev. Lett.*(2008), M. Roth [Pierre Auger Collaboration], *Proc. 30th ICRC, Mérida* (2007), arXiv:0706.2096v1 [astro-ph].
8. J. Abraham *et al.* [Pierre Auger Collaboration], *Nucl. Instrum. Methods* A **523**, 50 (2004).
9. X. Bertou *et al.* [Pierre Auger Collaboration], *Nucl. Instrum. Methods* A **568**, 839 (2006).
10. A. Etchegoyen [Pierre Auger Collaboration], arXiv:0710.1646 [astro-ph].
11. H.O. Klages [Pierre Auger Collaboration], *Proc. 30th ICRC, Mérida* (2007).
12. M. Ave [Pierre Auger Collaboration], *Proc. 30th ICRC, Mérida* (2007), arXiv:0709.2125v1 [astro-ph].
13. M. Unger *et al.*, *Nucl. Instrum. Methods* A **588**, 433 (2008).
14. H. Barbarosa *et al. Astropart. Phys.* **22**, 159 (2004)

15. T. Pierog *et al.*, *Proc. 30th ICRC, Mérida* (2007), arXiv:0802.1262 [astro-ph].
16. M. Nagano *et al. Astropart. Phys.* **22**, 235 (2004)
17. M. Ave *et al. Astropart. Phys.* **28**, 41 (2007)
18. D. Allard [Pierre Auger Collaboration], *Proc. 29th ICRC, Pune* **7**, 287 (2005).
19. P. Facal San Luis [Pierre Auger Collaboration], *Proc. 30th ICRC, Mérida* (2007), arXiv:0706.4322 [astro-ph].
20. L. Perrone [Pierre Auger Collaboration], *Proc. 30th ICRC, Mérida* (2007), arXiv:0706.2643 [astro-ph].
21. T. Yamamoto [Pierre Auger Collaboration], *Proc. 30th ICRC, Mérida* (2007), arXiv:0707.2638 [astro-ph].
22. J. Abraham *et al.* [Pierre Auger Collaboration], *Astropart. Phys.* **29**, 188 (2008); J. Abraham *et al.* [Pierre Auger Collaboration], *Science* **318**, 939 (2007). See also the contribution from A. Letessier-Selvon in these proceedings.
23. M. Unger [Pierre Auger Collaboration], *Proc. 30th ICRC, Mérida* (2007), arXiv:0706.1495v1 [astro-ph]. See also the contribution from J. Bellido in these proceedings.